Geochemistry Geophysics Geosystems G3

Article
Volume 13, Number 10
25 October 2012
Q10018, doi:10.1029/2012GC004190
ISSN: 1525-2027

Published by AGU and the Geochemical Society

Gas seepage and seismogenic structures along the North Anatolian Fault in the eastern Sea of Marmara

L. Gasperini, A. Polonia, and F. Del Bianco
Istituto di Scienze Marine-Consiglio Nazionale delle Ricerche, IT-40129 Bologna, Italy
(luca.gasperini@ismar.cnr.it)

G. Etiope
Istituto Nazionale di Geofisica e Vulcanologia, Sezione Roma 2, IT-00143 Rome, Italy

Faculty of Environmental Science and Engineering, Babes-Bolyai University, Cluj-Napoca 3400, Romania

G. Marinaro and P. Favali
Istituto Nazionale di Geofisica e Vulcanologia, Sezione Roma 2, IT-00143 Rome, Italy

F. Italiano
Istituto Nazionale di Geofisica e Vulcanologia, Sezione di Palermo, IT-90146 Palermo, Italy

M. N. Çağatay
General Geology Department, Mining Faculty, Istanbul Technical University, 34469 Istanbul, Turkey

[1] We carried out a combined geophysical and gas-geochemical survey on an active fault strand along the North Anatolian Fault (NAF) system in the Gulf of İzmit (eastern Sea of Marmara), providing for the first time in this area data on the distribution of methane (CH_4) and other gases dissolved in the bottom seawater, as well as the CH_4 isotopic composition. Based on high-resolution morphobathymetric data and chirp-sonar seismic reflection profiles we selected three areas with different tectonic features associated to the NAF system, where we performed visual and instrumental seafloor inspections, including in situ measurements of dissolved CH_4, and sampling of the bottom water. Starting from background values of 2–10 nM, methane concentration in the bottom seawater increases abruptly up to 20 nM over the main NAF trace. CH_4 concentration peaks up to ~120 nM were detected above mounds related probably to gas and fluids expulsion. Methane is microbial ($\delta^{13}C_{CH4}$: −67.3 and −76‰ versus VPDB), and was found mainly associated with pre-Holocene deposits topped by a 10–20 m thick draping of marine mud. The correlation between tectonic structures and gas-seepages at the seafloor suggests that the NAF in the Gulf of İzmit could represent a key site for long-term combined monitoring of fluid exhalations and seismicity to assess their potential as earthquake precursors.

Components: 9500 words, 11 figures, 2 tables.

Keywords: North Anatolian Fault; cold seeps; methane; seismogenic faults.

Index Terms: 1050 Geochemistry: Marine geochemistry (4835, 4845, 4850); 3075 Marine Geology and Geophysics: Submarine tectonics and volcanism.

Received 17 April 2012; **Revised** 25 September 2012; **Accepted** 25 September 2012; **Published** 25 October 2012.

Gasperini, L., A. Polonia, F. Del Bianco, G. Etiope, G. Marinaro, P. Favali, F. Italiano, and M. N. Çağatay (2012), Gas seepage and seismogenic structures along the North Anatolian Fault in the eastern Sea of Marmara, *Geochem. Geophys. Geosyst.*, *13*, Q10018, doi:10.1029/2012GC004190.

1. Introduction

[2] The association between submarine cold seeps and active fault systems may be identified thanks to a variety of different diagnostic sedimentary features, such as pockmarks, mud volcanoes, carbonate crusts or patches of reduced material at the seafloor [e.g., *Judd and Hovland*, 2007]. Gas seepage generally results from advective migration processes mainly driven by underground gas pressure gradients, gas buoyancy and fault-induced rock permeability, in turn determined by active tectonics [e.g., *Macgregor*, 1993; *Etiope and Martinelli*, 2002]. It has been suggested that gas migration and surface gas anomalies can increase substantially in connection with earthquakes [e.g., *Cicerone et al.*, 2009; *Heinicke et al.*, 2010]. Consequently, seismogenic faults may be privileged sites for observing surface gas anomalies potentially related to earthquakes [e.g., *Yang et al.*, 2010]. While interactions between fluids and crustal strain (seismic and aseismic) have been widely studied on land [e.g., *Muir-Wood and King*, 1993; *Trique et al.*, 1999], the importance of fluids in the dynamics of submarine faults has been recognized only recently, partly due to the progress of deep seafloor exploration [e.g., *Le Pichon et al.*, 1992; *Henry et al.*, 2002].

[3] Fluid outflow has been observed widely along active faults in the submerged portion of the North Anatolian Fault (NAF) northern strand (Figure 1), as seeps with large plumes [*Géli et al.*, 2008; *Bourry et al.*, 2009] or as carbonate crusts, black patches, and bacterial mats [e.g., *Armijo et al.*, 2005; *Zitter et al.*, 2008; *Géli et al.*, 2008]. Free gas emissions in the deep Marmara Basins appear also related to the occurrence of earthquakes [*Tary et al.*, 2011]. This has been observed, although qualitatively, in shallower areas such as the İzmit Gulf, along the NAF segment that ruptured during the 1999 İzmit earthquake [*Kuşçu et al.*, 2005]. However, studies addressing the tectonic control of seepage along active faults and temporal variations of gas releases in connection with the earthquake cycle are lacking.

[4] Due to its high geohazard potential, the Sea of Marmara has been identified as a unique natural laboratory to study relationships between fluids and seismicity through the EC funded ESONET-NoE (European Seas Observatory NETwork - Network of Excellence). Part of this project focused on the study of the İzmit Gulf, not far from the epicenters of the 1999 destructive earthquakes of İzmit and Duzce (M_w 7.4 and 7.2, respectively), which caused heavy damages and a large number of casualties.

[5] The main reason for focusing on this segment of the NAF is that the İzmit 1999 earthquake has caused an increase in tectonic loading that will be probably dissipated through a large earthquake close to Istanbul in the next decades [*Hubert-Ferrari et al.*, 2000; *Atakan et al.*, 2002; *Parsons et al.*, 2000].

[6] This paper reports on a combined geophysical/gas-geochemical investigation of tectonically active, seismogenic features in the Gulf of Izmit, along the submerged part of the NAF system, carried out in the frame of the MARMARA Demo Mission (DM) within the ESONET-NoE project [see *Géli et al.*, 2011]. In this area, gas-charged sediments are widespread, and gas emissions in correspondence to active seismogenic faults were inferred from acoustic images [*Polonia et al.*, 2002; *Kuşçu et al.*, 2005; *Gasperini et al.*, 2009].

[7] We first attempted to estimate the distribution of gas in the Holocene sediments using a close-spaced grid of high-resolution seismic data. We carried out extensive measurements of CH_4 dissolved in the seawater close to the seabed, coupled with visual inspections and the acquisition of other oceanographic data through a multiparametric towed vehicle equipped with CH_4 sensors. Bottom water samples were collected for dissolved gas analysis in different areas in the Gulf of Izmit (Figure 1), in the vicinity of tectonically driven seepages; moreover, as background references, we collected water samples far from known gas seeps (Figure 1).

[8] Our objective was to determine: (1) whether or not the gas emissions are associated with active tectonic structures; (2) what is the nature and source of the gas detected, sampled and analyzed in correspondence with those structures.

2. Structural Setting and Fluid Seepage

2.1. The North Anatolian Fault Below the Gulf of İzmit (Sea of Marmara)

[9] The NAF is a major continental transform system that extends E-W across Turkey for over 1600 km

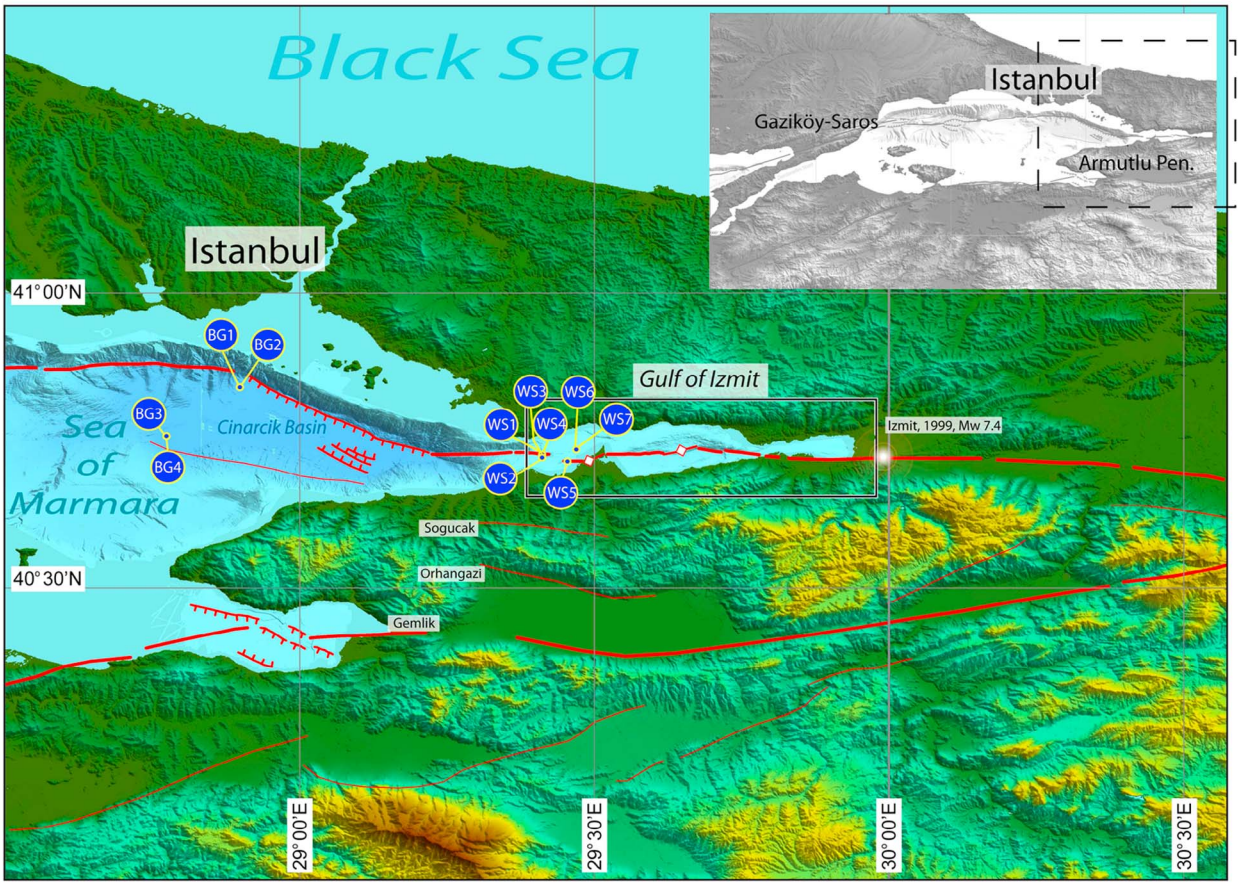

Figure 1. The North Anatolian Fault in the Sea of Marmara. Location of water samples are indicated by blue circles (BG = samples collected to determine background conditions; WS = samples collected over seep areas).

separating the Anatolian and Eurasian plates. The right-lateral, almost purely strike-slip tectonic regime that characterize the NAF over its eastern portion splays in the Sea of Marmara region into two major fault branches, about 100 km apart (Figure 1). The northern branch of the NAF, which accommodates over 80% of the Anatolia-Eurasia relative motion [*Armijo et al.*, 2002; *Meade et al.*, 2002], disappears below the Sea of Marmara close to the epicenter of the 1999 Izmit earthquake. Prior to 1999, marine geological data in the Sea of Marmara and in the Gulf of İzmit were scant, but after the İzmit earthquake, geophysical data, including high-resolution bathymetric maps and seismic reflection profiles, have been extensively collected as a consequence of the strong international effort that followed that disaster. A detailed morphotectonic map of the Gulf of İzmit (Figure 2), compiled using high-resolution multibeam echosounder and seismic reflection data [*Polonia et al.*, 2004], is among those results. It shows a complex pattern of releasing and restraining bends along the submerged trace of the NAF, causing the subsidence of three main basins separated by sills (Figure 2). In the İzmit Bay, the principal displacement zone of the NAF system forms a series of steps and ridges, oriented E-W (strike-slip), NW-SE (trans-tensional) and SW-NE (trans-pressional). This variety of structures is observed particularly in the center of the basins, and close to the Hersek Peninsula, where the deformation zone appears wider. At the entrance of the İzmit Gulf, the principal deformation zone converges again in a single narrow E-W oriented furrow (Figure 3a); as a rule, deformation zones are wider at the basin centers and narrower and more focused at their edges.

2.3. Seismicity and Cold Seeps

[10] The İzmit earthquake showed, although *ex post*, a strong correlation between a large seismic event and a sudden increase in fluid and gas emissions from the seafloor [*Kuşçu et al.*, 2005]. Repeated seismic reflection surveys in the Gulf of İzmit

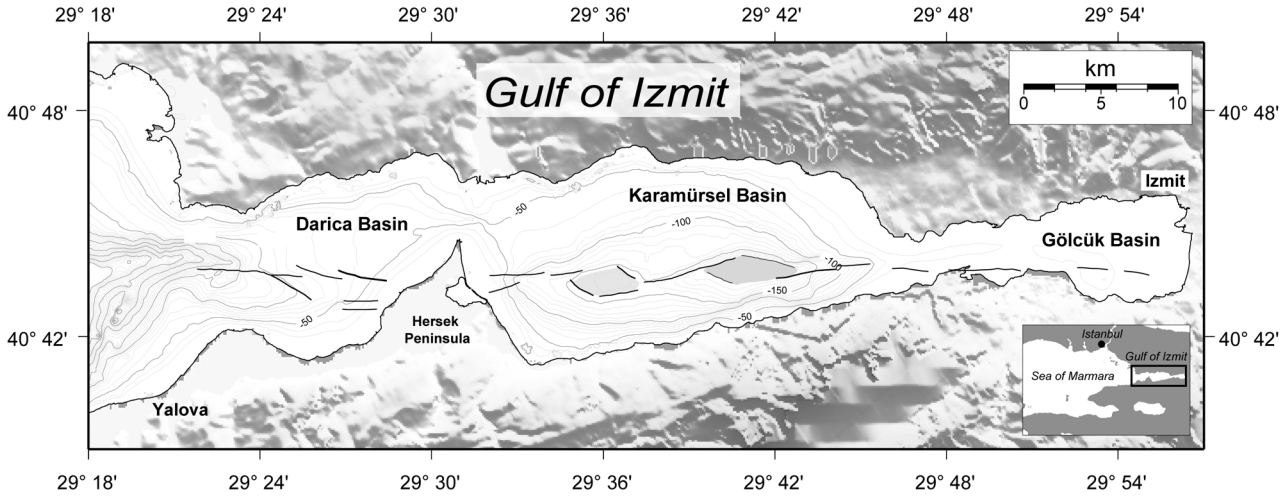

Figure 2. Simplified tectonic map of the İzmit Gulf. Darıca, Karamürsel and Gölcük basins are indicated, as well as the position of the principal deformation zone associated with the NAF system.

before and after the 17 August 1999 event revealed that the intensity of these emissions from the seafloor increased significantly after the earthquake and were still active several years later, although with decreased intensities [*Kuşçu et al.*, 2005; *Gasperini et al.*, 2011]. In these cases, gas emissions were detected by analyzing acoustic backscatter signals from different systems, including echo sounders and chirp-sonar profilers, as well as lower frequency seismic sources. The acoustic waves used to insonify the seafloor and sub-seafloor, ranging in frequency from few hundreds to tens of kHz, are scattered by gas bubbles in the water column, showing typical patterns in the records. Because these data are collected to image the seafloor (multi or single-beam echosounders, side-scan sonar systems) or the shallow sub-seafloor (chirp-sonar or sub-bottom profiling systems), correlating gas emissions with active tectonic structures becomes feasible. On the other hand, high-frequency (1–10 kHz) acoustic signals used to image the shallow sub-seafloor are very sensitive to the presence of gas in the sediments, that hamper the penetration in the sediments generating characteristic "blind" windows.

[11] We assessed the origin and the main pathways toward the surface of the gas seeps, and evaluated whether and where these seafloor emissions are controlled by tectonic deformations. Subsequently, the variability of fault-linked seepage and the main controlling factors should be assessed. This could be done by repeated surveys or, more effectively, by using multiparametric seafloor observatories [*Marinaro et al.*, 2006], able to monitor continuously different parameters including seismic activity, changes in gas concentrations in the seawater, current speed, pH, salinity, temperature, etc., over relatively long time spans (years). Actually, a multiparametric seafloor observatory (SN-4) was deployed in September 2009 and has been operative until October 2010,l within the MARMARA DM in the ESONET-NoE project [*Gasperini et al.*, 2009]. Results of this monitoring will be reported in another paper.

3. Methods

3.1. Geophysical Survey

[12] To compile a morphotectonic map of the study area, we used high-resolution multibeam bathymetry and shallow penetration seismic reflection profiles collected in the Sea of Marmara during three cruises onboard of R/V Urania (MARMARA-2001, -2005 and -2009; see cruise reports for more details at http://www.ismar.cnr.it/products/). Chirp data were collected using a 15 transducers Benthos Chirp II system. Processing and interpretation of the data, including reflectivity analysis and reflector picking

Figure 3. The Darıca Basin in the İzmit Gulf: (a) morphotectonic map with main fault segments and the three working areas (1, 2 and 3) indicated; (b) thickness of the Holocene deposits; (c) distribution of gas-bearing sediments (brown shading) from acoustic anomalies observed in chirp sonar profiles; red line indicates the location of chirp-sonar profile B1–30 shown in Figure 3.

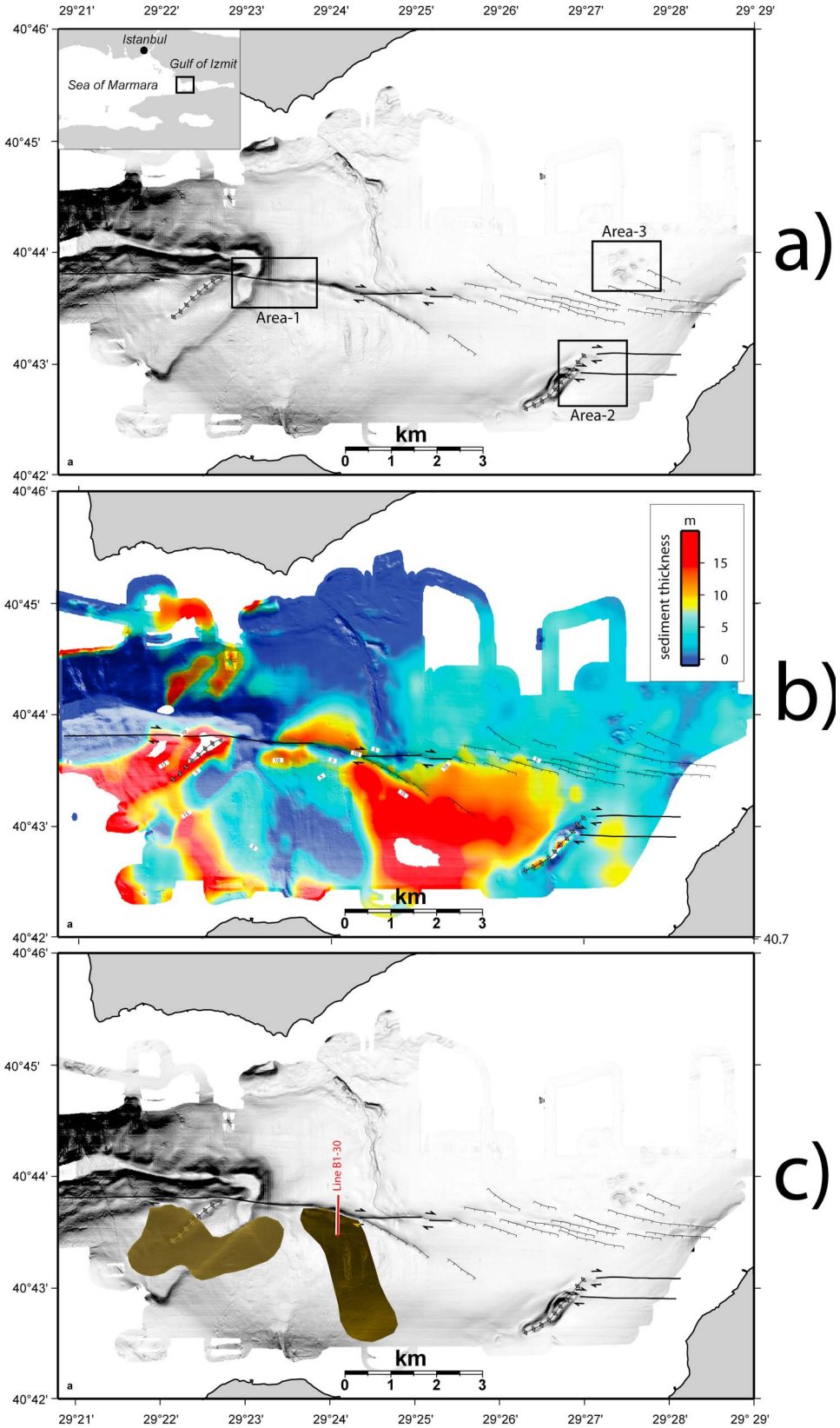
29°21'
29°22'
29°23'
29°24'
29°25'
29°26'
29°27'
29°28'
29° 29'
40°46'
40°45'
40°44'
40°43'
40°42'
Istanbul
Gulf of Izmit
Sea of Marmara
Area-1
Area-2
Area-3
km
0 1 2 3
a)
b)
c)
m
sediment thickness
15
10
5
0
Line B1-30
40.7

Figure 3

Table 1. Comparison of Dissolved Methane Concentrations Obtained by MEDUSA Sensors and Laboratory Analysis[a]

Site		CH_4 (nM) by GC	CH_4 (nM) by METS (Sensor 1)	CH_4 (nM) by HydroC (Sensor 2)
Area-1 (October 1)	Surface	10	0–5	20–25
	Bottom (WS3)	18	14–16	15–23
Area-2 (October 5)	Surface	nm	11–14	35–40
	Bottom (WS5)	23	15–20	20–30
Cast 3 (October 5)	Surface	8	0–5	25–30
	Bottom (WS6)	73	50–80	80–90

[a]"WS" refers to the water sample analyzed by GC and reported in Table 2; sensor data refer to the range observed in correspondence with water sampling; they are not the maximum values recorded (peaks shown in Figure 6); nm: not measured.

were carried out using the open-source software package SeisPrho [*Gasperini and Stanghellini*, 2009].

3.2. Visual Survey and Gas Detection

[13] We carried out the surveys using the deep-sea tow MEDUSA (Module for Environmental Deep UnderSea Applications), a cabled aluminum-frame module for casts and towed surveys ("flyovers") close to the seabed, equipped with modular scientific payloads [*Marinaro et al.*, 2011]. The instruments used in the Sea of Marmara included two independent methane sensors (the semiconductor METS by Franatech GmbH, Germany, and the optical HydroC by CONTROS Systems & Solutions GmbH, Germany), CTD and transmissometer (Seabird 19plus and Wet labs ECOBBRTD Deep Single Angle Scattering Meter), oxygen sensor (Optode 3830 Aanderaa), echo sounder (Tritech PA500–6), video camera and lights (Multi SeaCam 1060 - Deepsea Power&Light). The CH_4 METS sensor (Sensor 1) was calibrated in lab controlled conditions for a measuring range of 10–1,000 nM; it was post-calibrated (after the survey) and corrected taking into account the oxygen saturation. During the lab tests, the Sensor 1 did not show any significant drift. The CH_4 HydroC sensor (Sensor 2) was calibrated, in the same controlled conditions, for a range of 100–100,000 nM; it was not post-calibrated due to electronic failures, thus its data have been considered only as relative measures. The concentrations measured by both sensors were compared with laboratory gas-chromatograph (GC) analyses, as shown in Table 1; the GC analyses refer to water samples collected as described in section 3.3 and the corresponding methane sensor data are within the range of values shown during the water sampling events. However, methane sensor data are considered in semiquantitative terms (especially for Hydro-C sensor that had a calibration range higher than most of the observed CH_4 concentrations). This was considered satisfactory because, rather than the absolute values, we were interested in relative variations of the sensor signals during the horizontal "flyovers" close to the seabed. The results will show that Sensors 1 and 2, based on different gas detection techniques (semiconductor and optical), displayed exactly the same relative variations, i.e., simultaneous increases or decreases in the readings, proving their effectiveness in sensing CH_4 changes. The simultaneous CH_4 peaks, supported by GC analyses, were then used as indicators of gas seepage from the seabed. Detailed descriptions, performances and successful case histories of similar sensors are described in *Marinaro et al.* [2006], *Monteiro et al.* [2006], *Grunwald et al.* [2007], *Newman et al.* [2008], and *Krabbenhoeft et al.* [2010].

[14] During the survey, all data were displayed onboard by the MEDUSA control unit, which includes telemetry electronics and a PC for video and sensor data display. All measurements and visual recordings were carried out using a single time-base, to allow for correlations between different parameters and images, including those relevant to the system status, such as position and altitude.

3.3. Dissolved Gases

[15] Water samples for dissolved gas analyses were collected by Nansen bottles vertical casts and by the MEDUSA equipment. During the MEDUSA surveys, 2 surface and 7 bottom seawater samples were collected. The bottom samples were taken where the higher CH_4 signals were detected by MEDUSA sensors by a Tedlar® pipe with sampling inlet fixed close to the methane sensors and the video camera. At sites where the methane sensors indicated high CH_4 concentrations, bottom seawater was sampled using the following procedure: (1) using the pipe connected with MEDUSA, the bottom water was pumped onboard; (2) water was flushed through a gas separation chamber, and the gas cap was sniffed

by a portable CH_4 sensor (Metrex, Huberg, Italy; lower detection limit: 1 ppmv) in order to detect CH_4 increase; (3) once increasing CH_4 concentration were detected, the chamber was switched off-line, and the water samples collected and sealed in 250 ml Pyrex bottles, with a silicon septum held in place by an aluminum crimp-cap.

[16] Additional water samples were collected on board of the R/V Yunus S. using Nansen bottles, both close to the sea bottom in areas characterized by gas seepage, and in the western part of the Sea of Marmara, at fixed water depths of 100 and 500 m, to obtain a rough reference composition of the dissolved gases. Samples for dissolved gas analyses were stored in 250 ml glass bottles sealed on board by silicon/Teflon septa using special pliers. All samples suitable for both chemical and isotopic determinations, were collected taking care to prevent atmospheric contamination. Chemical analyses were carried out in the laboratory on the gas phase extracted after the attainment of equilibrium (at constant and known temperature) between the water sample and a known volume of host, high purity gas (argon), injected inside the sampling bottle (see for details: *Sugisaki and Taki* [1987] and *Capasso and Inguaggiato* [1998]).

[17] The analytical determination of He, H_2, O_2, N_2, CO, CH_4, CO_2 was carried out using a Perkin Elmer Clarus 500 gas chromatograph equipped with a double detector (TCD-FID; detection limits 1 ppm/vol), with argon as carrier gas.

[18] Helium isotope analyses were carried out on gas fractions extracted following the same procedure as for the gas chromatography. The sample was then purified following standard procedures [*Italiano et al.*, 2009]. Isotopic analyses of the purified helium fraction were performed by a static vacuum mass spectrometer (GVI5400TFT) that allows the simultaneous detection of ^3He and ^4He-ion beams, thereby keeping the $^3He/^4He$ error of measurement very low. Typical uncertainties in the range of low ^3He samples are within ±5%.

[19] Starting from the gas-chromatographic analyses, the composition of the dissolved gas phase was calculated taking into account the solubility coefficient of each gas (Bunsen coefficient "β," cc_{gas}/ml_{water} STP), the volume of gas extracted (cm^3) and the volume of the water sample, following equation (1):

$$G_C = \{[G_{gc}] * V\gamma_e + ([G_{gc}] * \beta_G * VW)\} \cdot VW^{-1} * V\gamma_e * V\gamma_i{}^{-1}/100 \quad (1)$$

where G_C is the concentration of the selected gas, G_{gc} is its concentration measured by the gas chromatograph (vol %), $V\gamma_e$ and $V\gamma_i$ represent the extracted and the introduced gas volumes respectively, while VW is the volume of the analyzed water sample [see *Italiano et al.* [2009] for further details).

[20] C_1-C_6 hydrocarbons, hydrogen (H_2) and stable carbon and hydrogen isotopic composition of CH_4 ($\delta^{13}C_{CH4}$ and δD_{CH4}) were analyzed by Isotech Labs Inc. Illinois, USA (Carle AGC 100–400 TCD-FID GC; precision 2%; 10% at the detection limit; Finnigan Delta Plus XL mass spectrometer, accuracy ±0.1‰); one sample was analyzed for δD_{CH4} at the Institute for Marine and Atmospheric Research Utrecht (CF-IRMS, Finnigan Delta Plus XL).

4. Results

4.1. Neo-tectonic Setting of the Darıca Basin

[21] The active tectonic features associated with the NAF in the Darıca Basin are shown in the morphobathymetric map of Figure 3a. The main fault track of the NAF intersects the Hersek Peninsula at 29°31′E (Figure 2). About 4 km east of this feature, at 29°34′E, the fault splays in two branches that cross the promontory at two different locations. To the West of the Hersek Peninsula, in the Darıca Basin, the deformation zone is broad and includes two different fault strands (Figure 3a); to the north, it is marked by a series of en-echelon segments around 1-km long. Displacement at each fault produces meter-high scarps cutting through the Holocene sediments. About 1 km to the south, a couple of E-W oriented strike-slip faults intersect a NE-SW topographic high that forms at a left-lateral step of the NAF (Figure 3a). W of the topographic high, the southernmost strike-slip fault merges to the main NAF at about 29°24′E. From this point to the W, the NAF principal deformation zone merges into a single strike-slip segment. Here, deformation appears to be localized within a relatively narrow zone (few tens of meters) showing almost pure strike-slip displacement. Toward the Çınarcık Basin to the W, the NAF parallel the south wall of a deeply eroded canyon (Figure 3a).

[22] The E-W oriented fault strands accommodate the strike-slip deformation while NW-SE oriented structures are mainly trans-tensional. Slip rate estimates show how the NW-SE oriented fault strand has similar horizontal and vertical slip rates (about 1 mm/yr), while the main E-W fault segment has

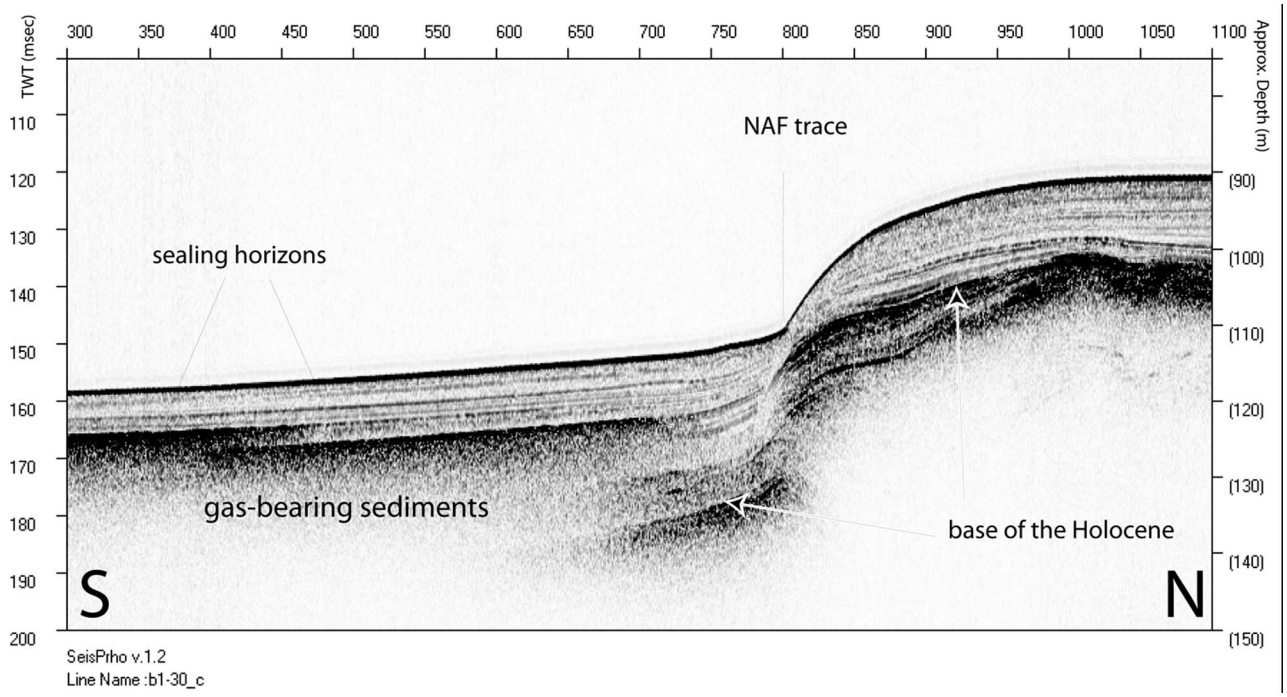

Figure 4. Chirp-sonar profile B1–30 crossing the principal displacement zone of the NAF in the Darıca Basin (see location in Figure 3). We note the upper transparent unit formed by Holocene fine-grained sediment locally permeated by upwelling gas from the lower lacustrine unit.

horizontal slip rate 8 to 9 times larger than vertical slip rate [*Polonia et al.*, 2004].

[23] Analysis of the high-resolution seismic profiles in the Darıca Basin reveals the presence of a transparent upper unit made of marine sediments deposited after the last post-glacial sea level rise (Figure 4). The character of the deposits below this Holocene unit is controlled by the −85 m isobaths, which corresponds to the Dardanelles sill. During MIS 3 and the main part of MIS 2 (from 60 to 15 ka BP), disconnection from the Mediterranean and Black seas, together with a dry climate resulted in a regression that transformed the Sea of Marmara into a brackish lake [*Çağatay et al.*, 2009; *Eriş et al.*, 2011]. The postglacial freshwater transgressive stage of the Marmara 'Lake' occurred between 15 and 13.5 ka B.P., leading to a rise in water level to −85 m by 13.0 ka BP [*Eriş et al.*, 2011]. During the initial stage of the Mediterranean ingression, the water level was at −85 m below its present level, with the development of shoreface deposits at that level [*Çağatay et al.*, 2003; *Polonia et al.*, 2004]. In the Darıca Basin, we observe that below the −85 m isobaths, the contact between lacustrine and marine Holocene deposits is conformable, while above this level it is constituted by a prominent erosional surface (Figure 4). Figure 3b shows the map of the Holocene deposit thickness, obtained by picking the reflector corresponding to the base of the Holocene and subtracting the water depth. The maximum thickness is located south of the NAF track, where a dip component of the NAF displaces the hanging wall by about 10 m.

[24] Analysis of seismic profiles determined the presence of gas pockets in the sediments. Depending on the sediment type and the gas concentration, gassy sediments may manifest as areas of: (1) acoustic "wipe outs" (very little signal returned as a result of acoustic attenuation); (2) acoustic turbidities (high amplitude scattering obscures any stratification); or (3) enhanced reflectors (amplitude of reflections from layers of sediment is strengthened) [*Judd and Hovland*, 1992; *Woodside et al.*, 1998]. The sedimentary sequence of the Darıca Basin is affected diffusely by the presence of gas. In the Holocene marine sequence, large wipe-out "windows" are visible, marked by a laterally sharp attenuation of sub-seafloor seismic reflections from the. The transparent sub-horizontal layers contain sealing horizons or capillary traps of gas in sand layers, that confine the gas in the subsurface; close to the active fault strands the gas in the Holocene deposits is less visible (Figure 4).

Table 2. Molecular and Isotopic Composition of Gas Extracted From Seawater Close to the Seabed From the Study Area (WS Samples) and From Marmara Seawater Far Away From the Seepage Area, Considered as a Possible "Local" Background (BG Samples)[a]

Site	Sample Depth Sample-Seafloor Distance[b] (m)	He	O_2	N_2	CH_4	CO_2	HS-CH_4[c]	$\delta^{13}C_{CH4}$	δD_{CH4}	R/R[d]	He/Ne
WS1 (area-1)	186; 1.5	2.4E-03	10	1455	39.2	33.6	nm	nm	nm	0.85	0.78
WS2 (area-1)	158; 1	2.2E-03	30	1505	22.8	38.2	nm	nm	nm	0.85	0.45
WS3 (area-1)	196; 1.5	9.8E-04	7	1455	17.4	32.9	nm	nm	nm	1.04	0.31
WS4 (area-1)	165; 1	1.4E-03	19	331	8.3	36.1	nm	nm	nm	1.05	0.40
WS5 (area-1)	56; 2	1.6E-03	22	338	7.8	33.1	nm	nm	nm	0.97	0.33
WS6 (area-2)	52; 6	1.0E-03	10	1380	22.8	35.6	0.03	−67.3	−145	1.16	0.30
WS7 (area-3)	51; 5		48	317	24.5	31.2	0.16	−76	−109	nm	nm
WS8 (area-3)	186; 1.5		59	443	69.9	47.9	nm	nm	nm	nm	nm
BG1	100; 1112		50	339	2.2	31.2	nm	nm	nm	nm	nm
BG2	500; 612		14	311	2.7	36.1	nm	nm	nm	nm	nm
BG3	100; 1098	1.4E-03	45	349	1.8	30.6	nm	nm	nm	0.99	0.38
BG4	500; 698		26	330	1.9	33.1	nm	nm	nm	nm	nm
ASSW		*1.8E-03*	*214*	*429*	*2.0*	*10.7*				*1.00*	*0.29*

[a] N_2, O_2 and CO_2 in μM; CH_4 in nM. Area-1, 2, 3 samples were collected on 1 and 5 October 2009, based on MEDUSA recordings. Samples for determining CH_4 in non-seepage areas (BG sites; March 2010) were collected both close to the seabed and at shallower depths. Concentrations of C_2-C_6 alkanes and H_2, not reported, were below the detection limit (see text); ASSW: Air Saturated Seawater, CH_4 concentration in equilibrium with the atmosphere, calculated for actual temperature and atmospheric CH_4 concentration.

[b] D: sample depth; d: sample distance from the seabed.

[c] methane concentration (% v/v) in the head-space extracted for isotopic analysis.

[d] $R/Ra = (^3He/^4He)_{sample}/(^3He/^4He)_{atmosphere;}$ $Ra = 1.39 \times 10^{-6}$; nm: not measured; bdl: below detection limits.

[25] We attempted to map these gas-bearing deposits using a close-space grid of high resolution seismic reflection profiles collected during several R/V Urania cruises. Figure 3c shows the distribution of observed gas-bearing sediments in the Holocene deposits of the Darıca Basin. We note a good fit between thickness of the Holocene deposits and the presence of gas in the sediments, with the NAF track separating gas-bearing deposits to the south from gas-free sediments to the north. This might suggest an important tectonic control on the Holocene depocenters and the presence of gas-bearing sediments along the NAF trace.

4.2. Dissolved Gases and Tectonic Features

[26] Morphobathymetric and seismic reflection data in the Darıca Basin enabled us to select three areas (*Area*-1 to -3 in Figure 3a) with gas seepages, in connection with tectonic features, have been investigated.

[27] A diffuse presence of gas seepages was observed in the Gulf of Izmit by *Kuşçu et al.* [2005] prior and after the 1999 Izmit earthquake through the analysis of seismic reflection profiles. However, this paper and other marine geological works published in this area did not report any data on gas geochemistry.

[28] We chose three study locations: (1) *Area*-1, western end of the Gulf of İzmit, where the principal deformation zone is narrow and offsets a marine canyon; (2) *Area*-2, a transpressive splay where a pressure-ridge forms; (3) *Area*-3, where a cluster of mounds located at the termination of *en-echelon* extensional fault segments emerge from the flat morphology. In each of these areas, we performed a MEDUSA survey, for a total of 32 h of video and data recording. Table 1 compares the CH_4 data recorded by the MEDUSA sensors with gas-chromatographic analyses. The composition of gas dissolved in seawater, as well as the CH_4 and He isotopic composition, are reported in Table 2.

[29] *Area*-1. Methane concentration in the surface seawater, analyzed by gas extraction from two samples collected in Area-1, was around 10 nM (Table 1), slightly above the theoretical air saturated seawater level (2 nM at surface seawater temperature). This is probably due to the diffuse hydrocarbon pollution (mainly from intense ship traffic) of this region. Lower values, up to 5 nM were recorded by the CH_4 METS sensor (Sensor 1, whose calibration range was however from 10 to 1000 nM). During the horizontal "flyovers" close to the seabed, Sensors 1 and 2 displayed exactly the same relative variations (i.e., simultaneous increasing or decreasing), which suggested real CH_4 changes. Close to

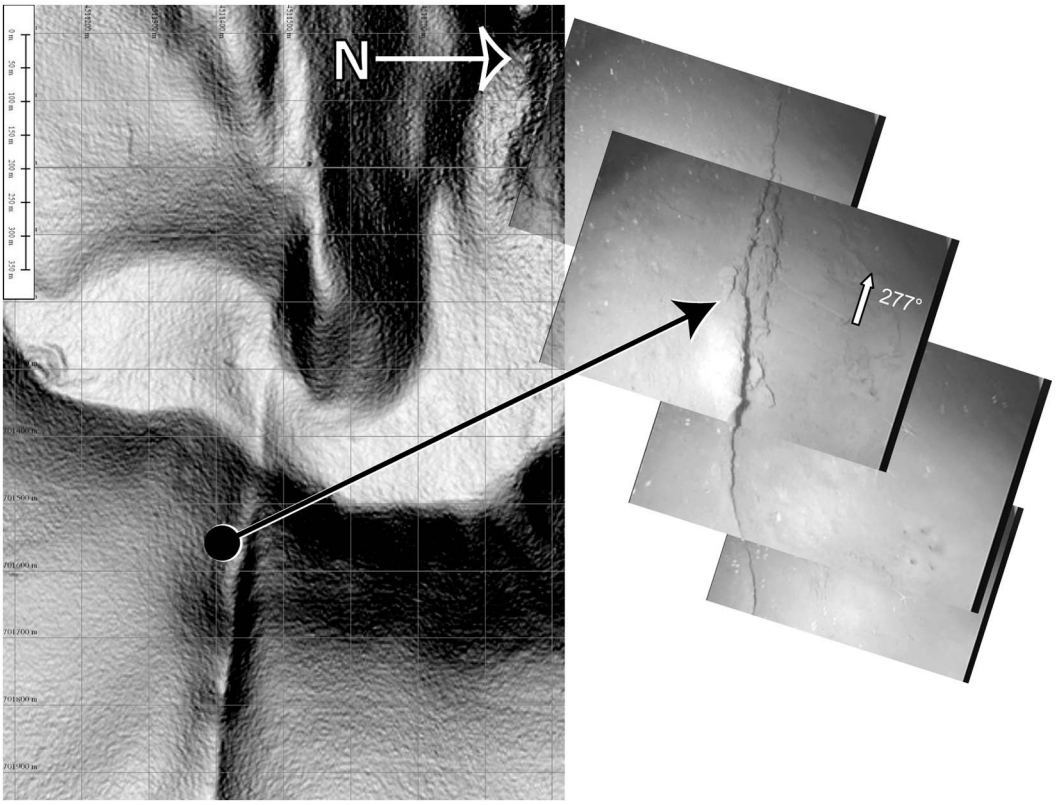

Figure 5. Surface rupture possibly related to the 1999 İzmit earthquake observed close to the western end of the Darıca Basin; (right) multibeam-derived slope map of the seafloor along the NAF trace; (left) photomosaic obtained by pictures collected by MEDUSA during the survey showing the surface rupture oriented at 277°.

the displaced canyon, at the entrance of the İzmit Gulf, a rectilinear fracture at the seafloor striking ≈277° was observed by the MEDUSA video camera (Figure 5). It was interpreted as the easternmost termination of the surface rupture caused by the 1999 İzmit earthquake [*Gasperini et al.*, 2011]. In correspondence with this fault zone, 0.5 to 2 m above the seafloor, peaks of CH_4 concentration were detected by both Sensors 1 and 2 (Figure 6, top): methane concentrations measured by Sensor 1 increased up to 20 nM. Up to 41 nM were measured by GC analysis (Table 2). N_2 concentrations were anomalously high, from 3 to 4 times the typical values of air saturated water. Other seawater parameters did not show significant changes: temperature was around 14.49°C, conductivity ∼4.645 S/m and oxygen constantly between 25,400 and 26,400 nM, indicating rather constant hypoxic conditions. Similar O_2 concentrations were measured by GC analysis (Table 2).

[30] Repeated passages over the fault zone with MEDUSA resulted in a map of methane concentrations close to the seafloor (Figure 7). In this map, that combines high-resolution morphobathymetry and CH_4 measurements close to the seafloor, "anomalous" concentrations of methane (i.e., >5 nM) are indicated by a color pattern (in red, the highest values). We observe that, although some spots of increased methane emission are present on both sides of the NAF main strand, maximum concentrations are centered on the principal deformation zone, marked as a narrow valley (Figure 7). Inside that canyon, displaced by the main track of the NAF, an offset of some tens of meters between the inferred fault trace and the maximum methane concentration is observed. This could be due either to the effect of bottom currents, which deviated the gas plume downstream in the canyon, or by non-coincidence between the maximum seepage flow and the fault. This latter is a common phenomenon due to the possible lower permeability of the fault gauges observed, for example, along the San Andreas fault in California, where gas seepage anomalies are located several meters southwest of the slip zone associated with the 1906 San Francisco earthquake [*King et al.*, 1996].

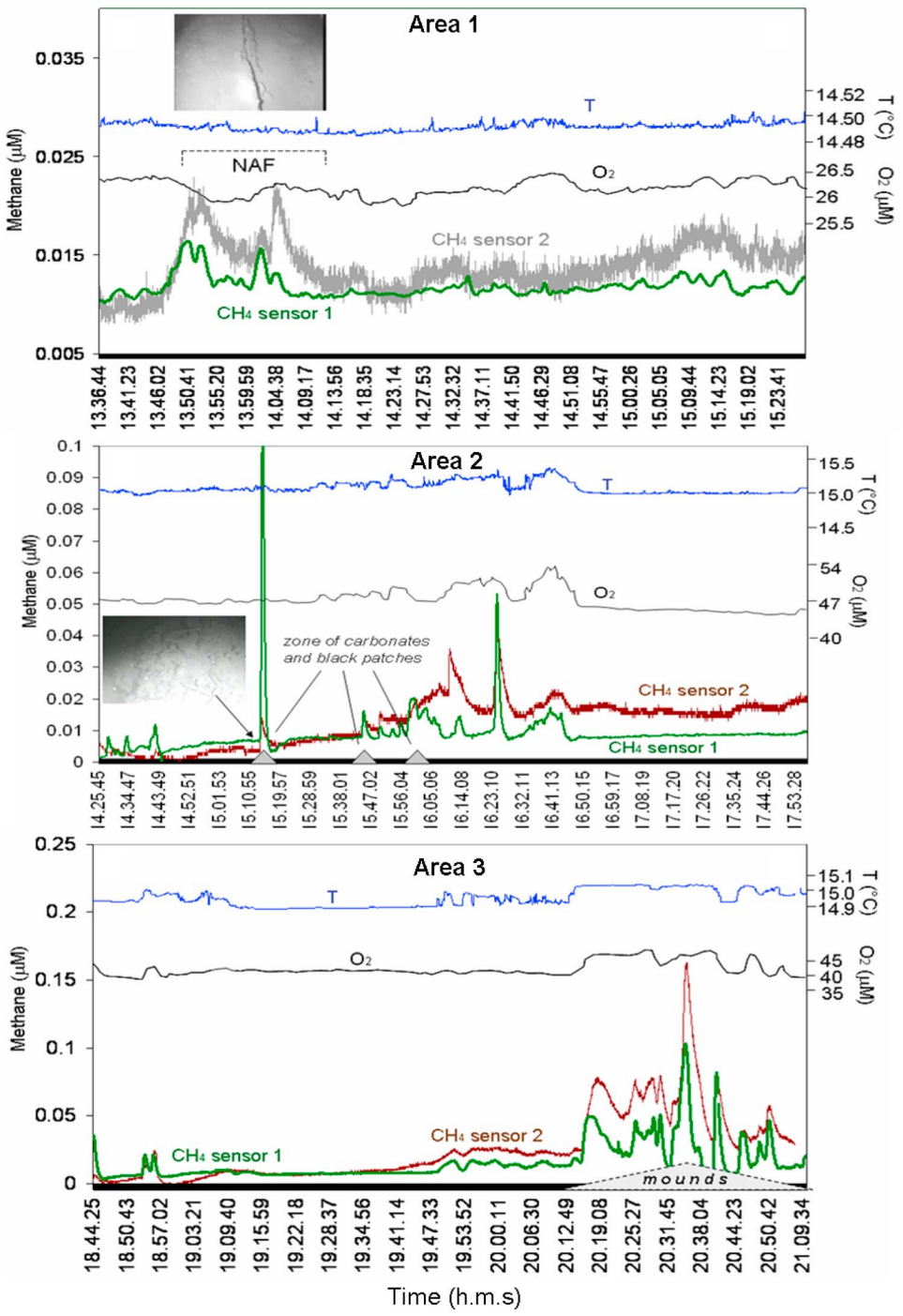

Figure 6. Horizontal variations of dissolved methane, temperature and oxygen detected close to the seabed (max. distance 3 m) by MEDUSA tow in the three surveyed areas (see acquisition pathway in the inset of Figure 9). Note the CH_4 peaks in correspondence with tectonic features.

[31] *Area*-2. A MEDUSA survey was carried out in *Area*-2 where the chirp-sonar profiles revealed acoustic images typical of bubble plumes in the water column (Figure 8). The maximum values of CH_4 in seawater were measured at the eastern edge of the pressure-ridge, at its intersection with a rectilinear strike-slip segment of the NAF. CH_4 concentration rose from about 5–10 nM to a peak of 105 nM (Figure 6, middle). In correspondence with the water sampling, methane sensors indicated levels of 10–15 nM (Sensor 1) and 20–30 nM (Sensor 2), compared with a GC analysis of 23 nM.

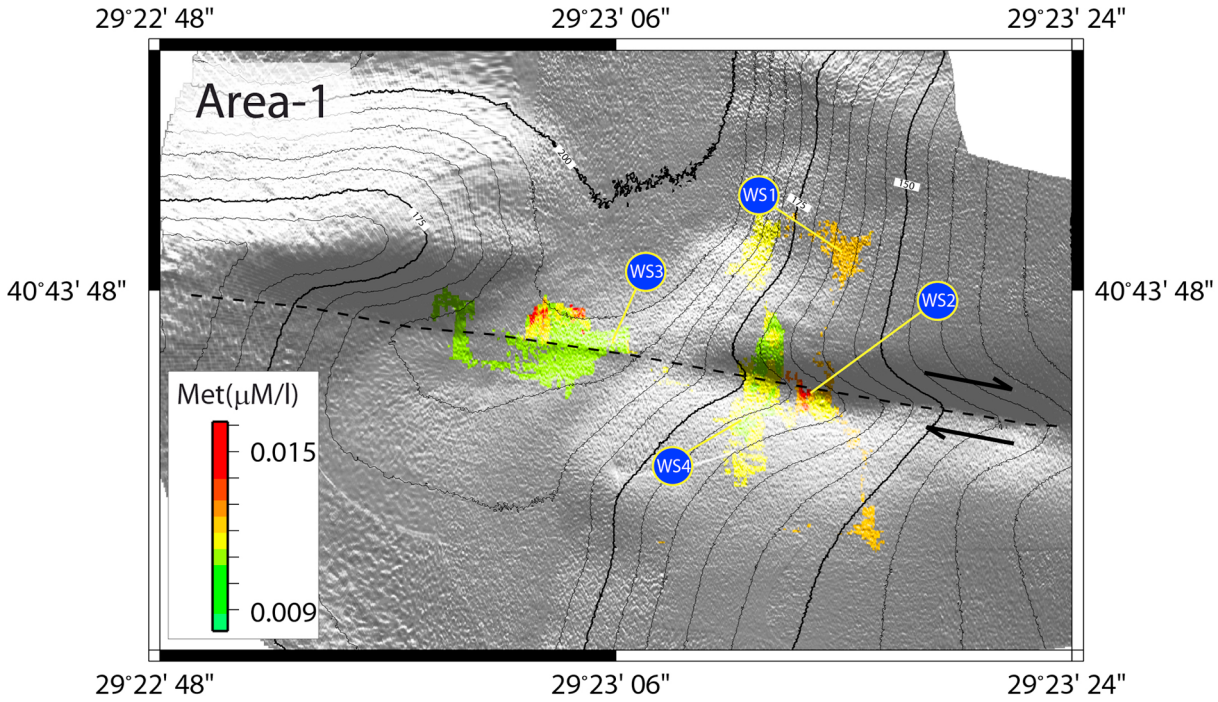

Figure 7. Seawater methane concentration close to the seafloor detected by MEDUSA Sensor 1 in *Area*-1. Anomalous CH_4 concentrations are represented by a color scale. Red values represent relative maxima. Note correlation between high CH_4 concentration and the trace of the NAF morphologically expressed by a narrow valley.

Isotopic analyses of CH_4 dissolved in a deep-water sample, 6 m from the seabed (Table 2) showed $\delta^{13}C$: −67.3‰ and δD: −145‰, which suggests a microbial origin. Oxygen concentrations are slightly higher than those in Area-1, but always in hypoxic range (<60,000 nM) as indicated by both the MEDUSA optode sensor and GC analyses (Figure 6 (top) and Table 2). N_2 concentrations are anomalously high as in Area-1.

[32] *Area*-3. Methane concentration in the bottom waters of Area-3, was generally below 10 nM (Figure 6, bottom). We performed several passages over the cluster of mounds located at the edge of a series of transtensive *en-echelon* faults in a relatively wide (some kms) deformation zone (Figure 9). In correspondence with the two largest mounds, methane concentration (Sensor 1) rose above 20 nM, with peaks up to 123 nM (Figures 6 (bottom) and 9). GC analysis of a water sample in this zone showed a CH_4 concentration of 73 nM, when the sensors indicated levels from 50 to 90 nM (Table 1). Isotopic analyses of CH_4 dissolved in a deep-water sample collected about 5 m over the seabed showed $\delta^{13}C$: −76‰ and δD: −109‰ (Table 2). Moreover, these values suggest a microbial origin for the gas emissions. Other seawater parameters (temperature, salinity and dissolved oxygen) did not show significant changes, if we exclude a slight increase of these parameters on top of each of the mounds. Hypoxic conditions were also observed in this area.

[33] Present-day seafloor conditions of the Gulf of Izmit, outlined by our combined acoustic and gas-geochemical observation, suggest the prevalence of diffusive degassing rather than the numerous intense gas plumes observed by *Kuşçu et al.* [2005] soon after the 1999 Izmit earthquake. In agreement with this, most of the seeps detected by MEDUSA were not visible in the sonic/ultrasonic profiles collected across the fault trace during the same cruise, except for the Area-2 site (Figure 8).

[34] In all the study areas (*Area*-1, 2 and 3), hydrocarbon alkanes heavier than methane and hydrogen were not detected in the gas extracted from the seawater, considering detection limits of 10 and 40 ppmv, respectively. Samples collected relatively far from the NAF strike-slip segments (BG) show methane concentrations consistent with atmospheric equilibrium (ASSW-Air-Saturated Sea Water, ∼2 nM). Oxygen values show significant hypoxia, with concentrations of 45,000–50,000 nM at 100 m w.d., decreasing to 14,000–25,000 nM at 500 m w.d., similar to that observed in the seepage areas. These data are consistent with those of previous CTD casts [*Henry et al.*, 2007; *Gasperini*

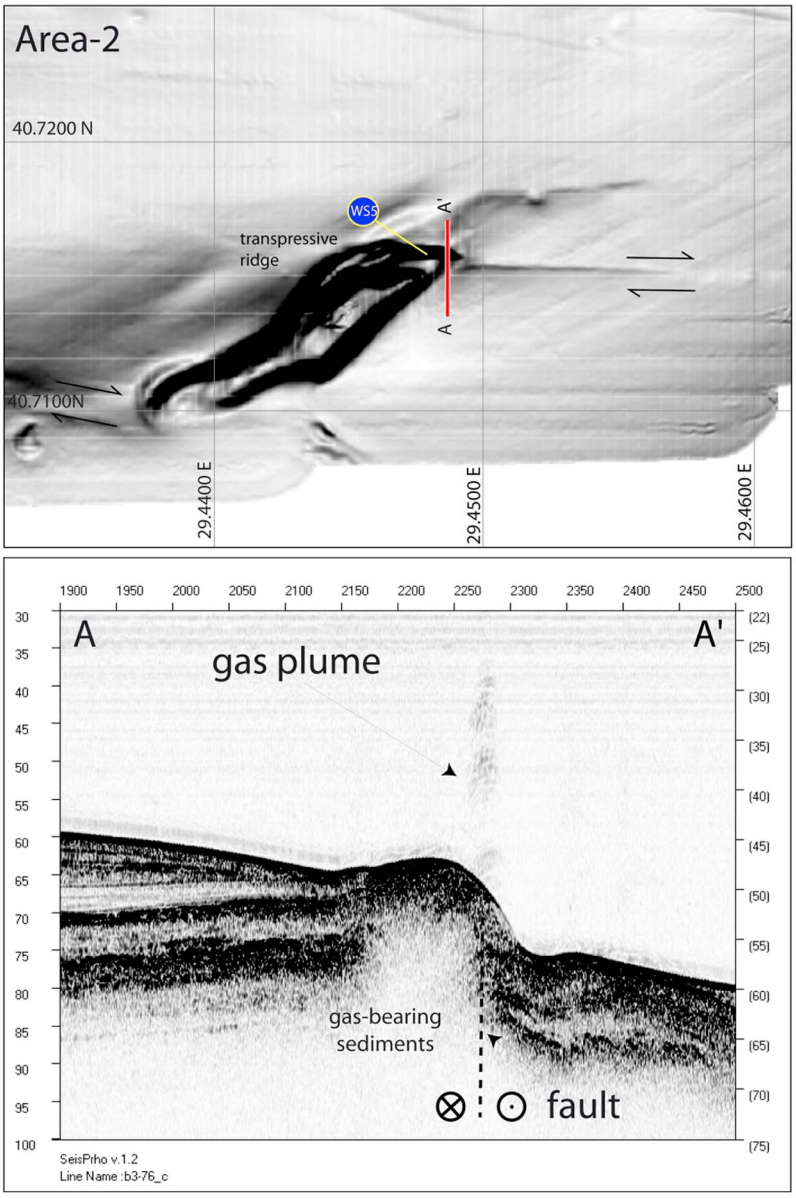

Figure 8. (top) Morphobathymetric map of the *Area*-2 showing the presence of a pressure-ridge at left-lateral overstep of the NAF. Location of Sample WS5 is indicated. (bottom) Chirp-sonar profile B3–76 (section A-A′) collected at the N edge of the pressure ridge showing the presence of gas in the water column and in the sediments. Geochemical data shown in Figure 6 for this area are also collected along this line.

et al., 2009; *Ritt et al.*, 2010], suggesting that deep water hypoxia is a widespread condition in the Sea of Marmara.

5. Discussion

[35] Our observations indicate that in the Darıca Basin, along the submerged portion of NAF that ruptured during the 1999 İzmit earthquake, methane concentration in the bottom seawater increases approaching the fault strands, both where fractures are observed at the seafloor, and where the fault is marked by a morphological scarp buried below hemipelagic sediments. Water samples collected above seafloor fractures (*Area*-1 and -2) and mounds (*Area*-3), display anomalous dissolved gas contents, with CH_4, N_2 and CO_2 concentrations well above the ASSW.

[36] Chemical analyses carried out on bottom water from the different areas (Table 2), show the presence

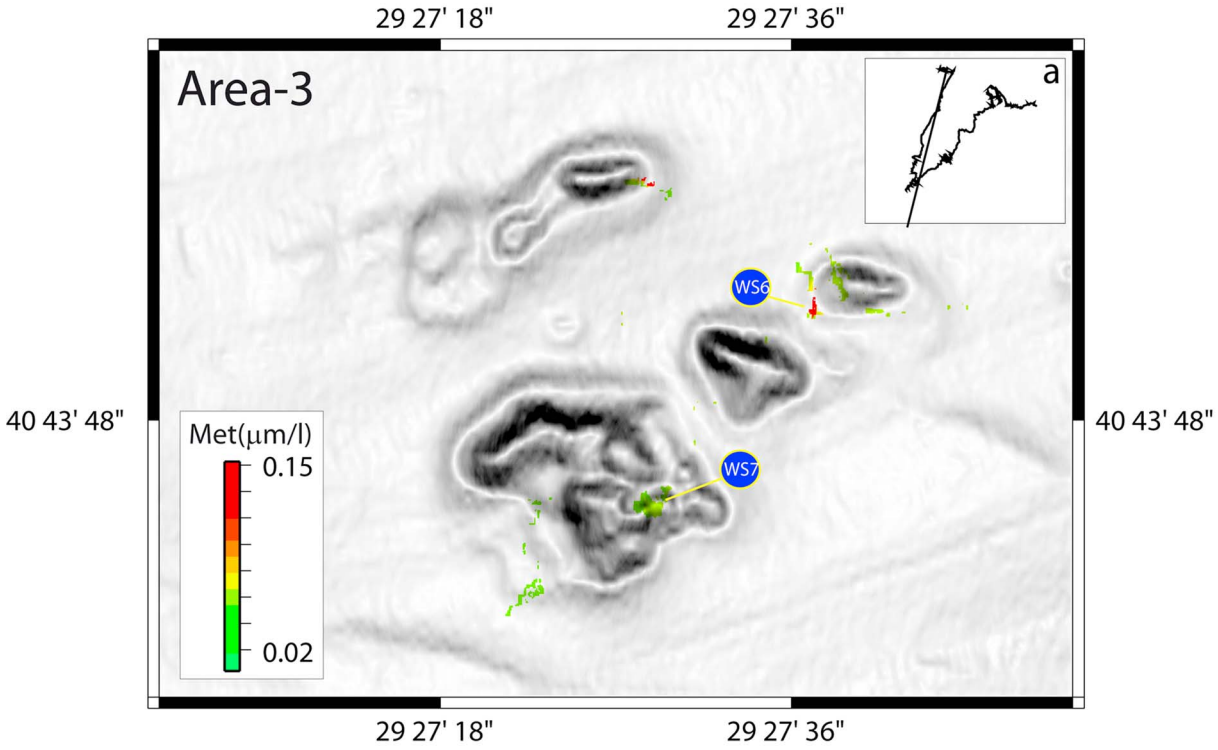

Figure 9. Morphobathymetric map of *Area*-3 showing the presence of mounds at the termination of en-echelon fault segments Seawater methane concentration close to the seafloor detected by MEDUSA Sensor 1 are represented by a color scale. The density of data acquisition is reported in the inset "a."

of N_2, O_2, CO_2, CH_4 which may have different origins (atmospheric and non-atmospheric). Although the atmospheric fraction, represented in the ternary diagram CH_4-O_2-CO_2 (Figure 10) by the oxygen vertex, is an obvious component of the dissolved gases, samples collected at depths of 100 and 500 m (BG1 to 4, Table 2) show CO_2 and O_2 contents three times higher and four/ten times lower than the

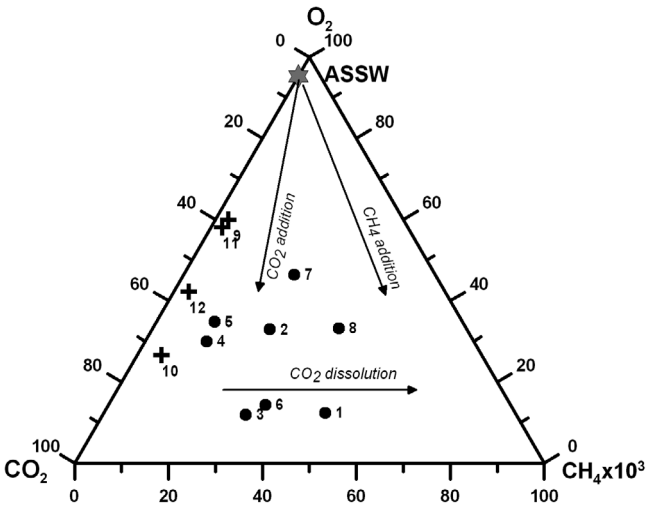

Figure 10. CH_4-O_2-CO_2 diagram. The triangular plot shows relative distribution of dissolved gas species for the collected samples. Samples from the Izmit Gulf (black filled circles) show that CO_2 and CH_4 addition to a typical ASSW (Air-Saturated Sea Water; gray star mark) may account for the detected gas composition. Reference samples for seawater far from the seepage areas (black crosses) show a low oxygen and the high CO_2 contents at the depth of 100 and 500 m. The occurrence of GWI (Gas-Water Interaction) processes may account for CO_2 loss (dissolution in seawater) from a probable deep-originated degassing. Samples labels as in Table 2.

ASSW, respectively. The triangular CH_4-O_2-CO_2 diagram of Figure 10 displays the relative concentrations of all samples. The background samples (BG) are clearly separated from samples collected over the gas seepage areas (1, 2 and 3), with a significant decrease in the O_2 content (<60,000 nM). This denotes a hypoxic condition for the Sea of Marmara poorly documented to date [*Henry et al.*, 2007; *Ritt et al.*, 2010].

[37] Geochemical features of the dissolved gases collected over the three investigated areas are interpreted as the result of several gas/water interaction processes (Gas-Water Interaction-GWI). CH_4 shows a clear microbial origin as in the nearby Çınarcık basin [*Bourry et al.*, 2009]. The isotopic ratio of hydrogen (δD_{CH4}) is relatively high, up to −109‰ VSMOW, in comparison with that typically reported for microbial gas. This could be due to methane oxidation, to be verified by further analyses.

[38] Comparing results obtained from the three areas, we observe that *Area*-1 and *2* show the same anomaly pattern, well correlated with tectonic structures, while *Area*-3, characterized by a more intense gas seepage and by the presence of fluid/sediment expulsion features (mounds), shows scattered (although relatively high) gas anomalies.

[39] The peculiar stratigraphy of the Gulf of Izmit basins suggests that the microbial CH_4 comes probably from pre-Holocene marine and lacustrine sediments accumulated below the −85 m isobaths, that represent the shoreface deposits of the earliest Holocene marine ingression [*Çağatay et al.*, 2003; *Polonia et al.*, 2004]. The clearest occurrence of gas in the sediments is found deeper than that shoreline deposits (Figure 3c). Below this stratigraphic level, we observe conformable marine deposits over lacustrine sediments, apparently not affected by subaerial erosion. From point to point, driven by fault ruptures that reach up to the seafloor in correspondence with the NAF principal displacement zone, buoyant gas appears to migrate to shallower level within the Holocene marine mud (Figure 4), which generally contains only a fraction of the gas present in the lacustrine deposits [*Peters et al.*, 2004].

[40] The excess of N_2 in samples with high CH_4 content (Table 2), could derive either from denitrification related to pollutants present in the seawater, or from the presence of methanotrophic bacteria [*Dekas et al.*, 2009]. The high CO_2 content of those waters (up to 46,000 nM, four times above the ASSW and higher than the average of background samples), suggests the possible presence of an additional gas source. Figure 10 shows the relative abundances of CH_4 and CO_2 and the distribution of our samples relative to a typical ASSW. Arrows in Figure 10 highlight the gas-water interactions phenomena, suggesting that a CO_2-dominated gas phase is released in addition to CH_4. The presence of endogenous CO_2, although not proved by our data, would agree with the CO_2-dominated composition of the gases released along the NAF onshore and with what was observed in cold and thermal springs on both the Northern and Southern strands of the NAF in the nearby Armutlu Peninsula [*Eisenlohr*, 1997; *Balderer et al.*, 2002; *de Leeuw et al.*, 2010] and in the Gaziköy-Saros segment [*Doğan et al.*, 2009]. As observed by *Doğan et al.* [2009] along four transects across the NAF on the western (Izmit) and eastern (Gaziköy-Saros) sides of the Marmara Basin, CO_2 is degassed from the soil and dissolves in the water with an isotopic signature not correlated with the CO_2 efflux values, suggesting that the CO_2 efflux anomaly is caused by a biogenic gas flow, possibly controlled by the tectonic deformations.

[41] Helium isotopic ratios in the Marmara basin display crustal values to the East, and magmatic ratios to the West [*Doğan et al.*, 2009], confirming that the fault plays an important role in transferring deep-origin gas to the surface.

[42] The isotopic composition of helium dissolved in the background (BG3) denotes an atmospheric origin, also confirmed by the He concentration, although the measured $^4He/^{20}Ne$ ratio (0.38) is above the ASSW value of 0.285 [*Mamyrin and Tolstikhin*, 1984]. Conversely, $^4He/^{20}Ne$ ratios higher than the ASSW are detected in samples from the seepage areas (WS1, WS2, Table 2); they show a helium content 30% above the BG and a slight ^4He contribution, that drops the atmospheric $^3He/^4He$ ratio to 0.78–0.85Ra (Table 2).

[43] On the R/Ra versus $^4He/^{20}Ne$ graph (Figure 11) our seafloor samples are plotted together with onshore data and theoretical mixing lines between atmospheric and mantle/crustal components. The mixing lines are built assuming the atmospheric component (as ASSW) marked by $^3He/^4He = 1.39 \times 10^{-6}$ and $^4He/^{20}Ne = 0.285$, the crustal-type component with 0.02Ra and 0.5Ra with $^4He/^{20}Ne = 1000$ [*Sano and Wakita*, 1985] and mantle-type components as MORB-type mantle with 8Ra and $^4He/^{20}Ne = 1000$ [e.g., *Hilton et al.*, 1998] and a possible mantle "contaminated" by crustal products assumed to have $^3He/^4He$ in the range of 2.5Ra and

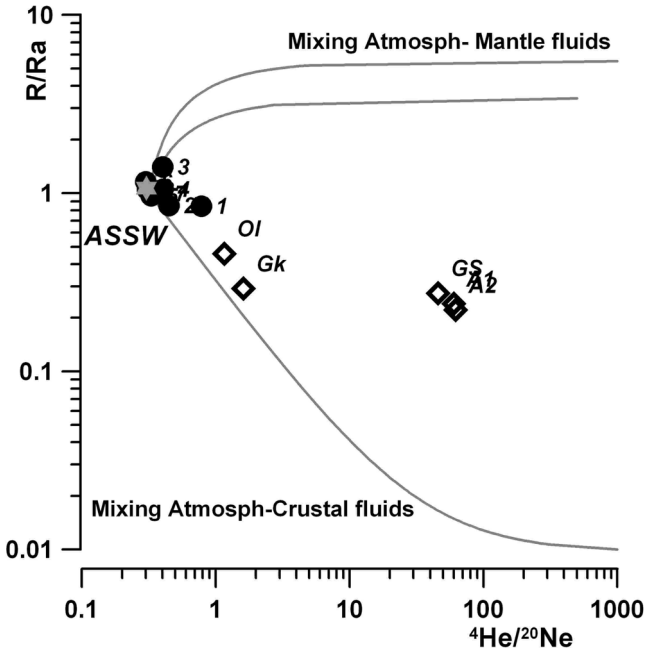

Figure 11. $^{3}He/^{4}He$ vs $^{4}He/^{20}Ne$ ratios. The empty circles mark the collected samples. Sample identification by numbers (as in Table 2 without WS). As expected, the measured isotopic ratios fall close the ASSW typical signature. Values recorded on samples from the nearby land used as reference (empty diamonds, triangles and squared symbols from *Eisenlohr* [1997] and *Doğan et al.* [2009]) show that the two dissolved gases (samples WS1 and WS2) marked by ^{4}He enrichment and higher $^{4}He/^{20}Ne$ ratios relative to ASSW, can be considered as a mixture of different sources (air and crustal-derived). $^{3}He/^{4}He$ ratios are expressed as R/Ra notation where R is the sample helium isotopic ratio and Ra is the atmospheric $^{3}He/^{4}He = 1.39 \times 10^{-6}$. Labels for in-land samples, gray triangle mark (data after *Eisenlohr* [1997]): OI = Orhangazi Ilipinar; GS = Sogucak; A1/2 = Armutlu area; GK Gemlik. Black squared mark = samples from the area of Ganos fault (data after *Doğan et al.* [2009]); Grey crosses marks (data after *Doğan et al.* [2009]): samples from Istanbul and Armutlu areas.

$^{4}He/^{20}Ne = 500$. The plot of our samples shows the presence of a crustal component (^{4}He enrichment) for WS1 and WS2, in agreement with data from spring samples collected close the Izmit-Sapanca fault to the East (Armutlu Peninsula, Izmit area, Istanbul area), and the Gazikoy-Saros fault to the West [*Eisenlohr*, 1997; *Doğan et al.*, 2009]. This sample distribution is interpreted as a binary mixing of atmospheric source and helium from the same crustal component feeding the in-land manifestations [*Eisenlohr*, 1997; *Doğan et al.*, 2009].

[44] As reported by *Doğan et al.* [2009], helium isotopic ratios exhibit changes probably related to the 1999 Izmit earthquake, and increased CO_2 effluxes are detected in coincidence of the NAF across the Izmit Gulf. A similar degassing activity might occur beneath the sedimentary layers of the Marmara seabed, where methane is produced. Mantle-derived helium has recently been detected in the hydrocarbon seeps of western Sea of Marmara [*Burnard et al.*, 2012], confirming the deep-crustal and gas bearing nature of the NAF in this region.

[45] Due to the high CO_2 solubility in seawater (3.5 g L^{-1}_{H2O} STP), three orders of magnitude larger than CH_4 (22.7×10^{-3} g L^{-1}_{H2O} STP [*Weiss*, 1974]), the former is mostly lost during its ascent through seawater-saturated sediments and close to the seabed. However, as the vertical permeability changes in response to lithospheric stresses during a major earthquake, changes in both the flow regime and gas composition could take place, and possibly detected at the seafloor. Accumulation of tectonic stress on the active segment of the NAF below the Sea of Marmara might change the shallow versus deep ratio of the released fluids, as observed in other sites in different geodynamic settings [e.g., *Italiano et al.*, 2004].

6. Conclusions

[46] Multidisciplinary geophysical/gas-geochemical survey of the Darıca Basin, in the Gulf of İzmit (Eastern Sea of Marmara), close to the western termination of the surface rupture generated by the 1999

İzmit earthquake, verified a correlation between tectonic structures and gas-seepages at the seafloor. Data analysis suggests that: gas-bearing sediments are common in the Gulf of İzmit, particularly below the −85 m isobaths; tectonic deformations control the distribution of gas in the sediments by confining gas pockets, or by creating preferential gas-escape pathways; for this reason, the seepage of gas from the subsurface is almost invariably connected to the presence of tectonic structures, being the relatively thick carpet of Holocene deposits an effective sealing cap; a strong correlation links tectonic structures and methane concentration in bottom seawater, with anomalies up to 2 orders of magnitude above background (>100 nM); over the same structures, geochemical features of dissolved gas in the bottom waters suggest the release of a gas phase composed by locally produced microbial CH_4 and a possible crustal CO_2 contribution, which has been observed along the onshore section of the NAF.

[47] These observations indicate that combining geologic and geochemical/oceanographic studies could improve our knowledge on the tectonic activity of the NAF; moreover, they suggest that tectonic-related gas seeps, particularly active during large earthquakes (e.g., the 1999 Mw 7.4 Izmit earthquake) are persistent, although probably weaker, for long times (up to tens of years) after the events. For this reason, and because these features appear confined along the principal displacement zone of the NAF, locally very narrow, they are considered interesting sites for long-term monitoring of fluid exhalations as earthquake precursor signals.

Acknowledgments

[48] We thank Captain and crew of cruises MARMARA - 2009, 2010, 2011, onboard of R/V Urania. The MARMARA-2009 cruise was partially funded by MARMARA DM coordinated by Louis Géli within the activities of the ESONET-NoE EC project. Thanks are due to Giovanni Bortoluzzi who helped in many ways during acquisition and processing of the data, Ivan Vigano (Institute for Marine and Atmospheric Research Utrecht) for CH_4 isotopic analyses, and Enrico Bonatti for a final review of the manuscript. Most of the maps were compiled using GMT software [*Wessel and Smith*, 1998]. The comments/suggestions of an anonymous referee, Pierre Henry and the Editor of G-cubed, Thorsten Becker, greatly improved the quality of the manuscript.

References

Armijo, R., B. Meyer, S. Navarro, G. King, and A. A. Barka (2002), Asymmetric slip partitioning in the Sea of Marmara pull-apart: A clue to propagation processes of the North Anatolian Fault?, *Terra Nova*, *14*, 80–86, doi:10.1046/j.1365-3121.2002.00397.x.

Armijo R., et al. (2005), Submarine fault scarps in the Sea of Marmara pull-apart (North Anatolian Fault): Implications for seismic hazard in Istanbul, *Geochem. Geophys. Geosyst.*, *6*, Q06009, doi:10.1029/2004GC000896.

Atakan, K., A. Ojeda, M. Meghraoui, A. A. Barka, M. Erdik, and A. Bodare (2002), Seismic Hazard in Istanbul following the 17 August 1999 İzmit and 12 November 1999 Düzce Earthquakes, *Bull. Seismol. Soc. Am.*, *92*, 466–482, doi:10.1785/0120000828.

Balderer, W., F. Leuenberger, F. Suner, T. Yalcin, and W. Stichler (2002), Effects of the Cinarcik-Ismit August 17, 1999 earthquake on the composition of thermal and mineral waters as revealed by chemical and isotope investigations, *Geofis. Int.*, *41*, 385–391.

Bourry, C., B. Chazallon, J. L. Charlou, J. P. Donval, L. Ruffine, P. Henry, L. Géli, M. N. Çağatay, S. Inan, and M. Moreau (2009), Free gas and gas hydrates from the Sea of Marmara, Turkey Chemical and structural characterization, *Chem. Geol.*, *264*, 197–206, doi:10.1016/j.chemgeo.2009.03.007.

Burnard, P., S. Bourlange, P. Henry, L. Géli, M. D. Tryon, B. Natalin, A. M. C. Sengör, M. S. Özeren, and M. N. Çagatay (2012), Constraints on fluid origins and migration velocities along the Marmara Main Fault (Sea of Marmara, Turkey) using helium isotopes, *Earth Planet. Sci. Lett.*, *341–344*, 68–78, doi:10.1016/j.epsl.2012.05.042.

Çağatay, M. N., N. Görür, A. Polonia, E. Demirbag, M. Sakinc, M.-H. Cormier, L. Capotondi, C. McHugh, O. Emre, and K. Eriş (2003), Sea level changes and depositional environments in the İzmit Gulf, eastern Marmara Sea, during the late glacial-Holocene period, *Mar. Geol.*, *202*, 159–173, doi:10.1016/S0025-3227(03)00259-7.

Çağatay, M. N., et al. (2009), Late Pleistocene-Holocene evolution of the northern shelf of the Sea of Marmara, *Mar. Geol.*, *265*, 87–100, doi:10.1016/j.margeo.2009.06.011.

Capasso, G., and S. Inguaggiato (1998), A simple method for the determination of dissolved gases in natural waters. An application to thermal waters from Vulcano island, *Appl. Geochem.*, *13*(5), 631–642, doi:10.1016/S0883-2927(97)00109-1.

Cicerone, R. D., J. E. Ebel, and J. Britton (2009), A systematic compilation of earthquake precursors, *Tectonophysics*, *476*, 371–396, doi:10.1016/j.tecto.2009.06.008.

Dekas, A. E., R. S. Poretsky, and V. J. Orphan (2009), Deep-sea archaea fix and share nitrogen in methane-consuming microbial consortia, *Science*, *326*, 422–426, doi:10.1126/science.1178223.

de Leeuw, G. A. M., D. R. Hilton, N. Gulec, and H. Mutlu (2010), Regional and temporal variations $CO_2/^3He$, $^3He/^4He$ and $\delta^{13}C$ along the North Anatolian Fault Zone, Turkey, *Appl. Geochem.*, *25*, 524–539, doi:10.1016/j.apgeochem.2010.01.010.

Doğan, T., H. Sumino, K. Nagao, K. Notsu, M. K. Tuncer, and C. Çelik (2009) Adjacent releases of mantle helium and soil CO_2 from active faults: Observations from the Marmara region of the North Anatolian Fault zone, Turkey, *Geochem. Geophys. Geosyst.*, *10*, Q11009, doi:10.1029/2009GC002745.

Eisenlohr, T. (1997), The thermal springs of the Armutlu Peninsula (NW turkey) and their relationship to geology and tectonic, in *Active Tectonics in Northwestern Anatolia, The Marmara Poly Project, Switzerland (CHE): V/d/f*, edited by C. Schindler and M. Pfister, pp. 197–228, CHE, Zurich, Switzerland.

Eriş, K. K., M. N. Çağatay, S. Akcer, L. Gasperini, and Y. Mart (2011), Late glacial to Holocene sea-level changes in the Sea of Marmara: New evidence from high-resolution seismic and core studies, *Geo Mar. Lett.*, *31*, 1–18, doi:10.1007/s00367-010-0211-1.

Etiope, G., and G. Martinelli (2002), Migration of carrier and trace gases in the geosphere: An overview, *Phys. Earth Planet. Int.*, *129*(3–4), 185–204.

Gasperini, L., and G. Stanghellini (2009), SeisPrho: An interactive computer program for processing and interpretation of high-resolution seismic reflection profiles, *Comput. Geosci.*, *35*, 1497–1507, doi:10.1016/j.cageo.2008.04.014.

Gasperini, L., L. Géli, P. Favali, M. N. Çağatay, and N. Görür (2009), MARM2009: Marine geological study of the North-Anatolian Fault beneath the Sea of Marmara. Cruise Report, technical report, ISMAR-CN, Bologna, Italy. [Available at http://www.ismar.cnr.it/prodotti/reports-campagne/2000–2009.]

Gasperini, L., A. Polonia, P. Henry, X. Le Pichon, G. Bortoluzzi, and M. Tryon (2011), How far did the surface rupture of the 1999 İzmit earthquake reach in Sea of Marmara?, *Tectonics*, *30*, TC1010, doi:10.1029/2010TC002726.

Géli, L., et al. (2008), Gas emissions and active tectonics within the submerged section of the North Anatolian Fault zone in the Sea of Marmara, *Earth Planet. Sci. Lett.*, *274*, 34–39, doi:10.1016/j.epsl.2008.06.047.

Géli, L., N. Cagatay, P. Henry, L. Gasperini, P. Favali, and G. Cifci (2011), Towards permanent, multi-disciplinary sea-floor observatories in the Sea of Marmara: Results from the Marmara Demonstration Mission of ESONET/NoE, paper presented at IEEE Symposium/Workshop on Scientific Use of Submarine Cables and Related Technologies, Tokyo.

Grunwald, M., O. Dellwig, G. Liebezeit, B. Schnetger, R. Reuter, and H. J. Brumsack (2007), A novel time-series station in the Wadden Sea (NW Germany): First results on continuous nutrient and methane measurements, *Mar. Chem.*, *107*, 411–421, doi:10.1016/j.marchem.2007.04.003.

Heinicke, J., F. Italiano, U. Koch, G. Martinelli, and L. Telesca (2010), Anomalous fluid emission of a deep borehole in a seismically active area of Northern Apennines (Italy), *Appl. Geochem.*, *25*, 555–571, doi:10.1016/j.apgeochem.2010.01.012.

Henry, P., S. Lallemant, K. Nakamura, U. Tsunogai, S. Mazzotti, and K. Kobayashi (2002), Surface expression of fluid venting at the toe of the Nankai wedge and implications for flow paths, *Mar. Geol.*, *187*(1–2), 119–143, doi:10.1016/S0025-3227(02)00262-1.

Henry, P., T. A. Zitter, X. Le Pichon, C. A. Sengor, N. Gorur, L. Gasperini, L. Géli, M. D. Tryon, and the Shipboard Scientific Party MarNaut Cruise (2007), Manned submersible observations at cold seeps in the North Anatolian Fault zone, Sea of Marmara, *Eos Trans. AGU*, *88*(52), Fall Meet. Suppl., Abstract B54C-01.

Hilton, D. R., K. Gronvold, A. E. Sveinbjornsdottir, and K. Hammerschmidt (1998), Helium isotope evidence for off-axis degassing of the Icelandic hotspot, *Chem. Geol.*, *149*, 173–187, doi:10.1016/S0009-2541(98)00044-8.

Hubert-Ferrari, A., A. A. Barka, E. Jacques, S. S. Nalbant, B. Meyer, R. Armijo, P. Tapponier, and G. C. P. King (2000), Seismic hazard in the Marmara Sea region following the 17 August 1999 İzmit earthquake, *Nature*, *404*, 269–273, doi:10.1038/35005054.

Italiano, F., G. Martinelli, and A. Rizzo (2004), Geochemical evidence of seismogenic-induced anomalies in the dissolved gases of thermal waters: A case study of Umbria (Central Apennines, Italy) both during and after the 1997–1998 seismic swarm, *Geochem. Geophys. Geosyst.*, *5*, Q11001, doi:10.1029/2004GC000720.

Italiano, F., P. Bonfanti, M. Ditta, R. Petrini, and F. Slejko (2009), Helium and carbon isotopes in the dissolved gases of Friuli region (NE Italy): Geochemical evidence of CO_2 production and degassing over a seismically active area, *Chem. Geol.*, *266*, 76–85, doi:10.1016/j.chemgeo.2009.05.022.

Judd, A. G., and M. Hovland (1992), The evidence of shallow gas in marine-sediments, *Cont. Shelf Res.*, *12*, 1081–1095, doi:10.1016/0278-4343(92)90070-Z.

Judd, A. G., and M. Hovland (2007), *Seabed Fluid Flow: Impact on Geology, Biology and the Marine Environment*, 442 pp., Cambridge Univ. Press, Cambridge, U. K., doi:10.1017/CBO9780511535918.

King, C. Y., B. S. King, W. C. Evans, and W. Zhang (1996), Spatial radon anomalies on active faults in California, *Appl. Geochem.*, *11*, 497–510, doi:10.1016/0883-2927(96)00003-0.

Krabbenhoeft, A., G. L. Netzeband, J. Bialas, and C. Papenberg (2010), Episodic methane concentrations at seep sites on the G.L. upper slope Opouawe Bank, southern Hikurangi Margin, New Zealand, *Mar. Geol.*, *272*, 71–78, doi:10.1016/j.margeo.2009.08.001.

Kuşçu, I., M. Okamura, H. Matsuoka, E. Gokasan, Y. Awata, H. Tur, and M. Simsek (2005), Seafloor gas seeps and sediment failures triggered by the August 17, 1999 earthquake in the Eastern part of the Gulf of İzmit, Sea of Marmara, NW Turkey, *Mar. Geol.*, *215*, 193–214, doi:10.1016/j.margeo.2004.12.002.

Le Pichon, X., K. Kobayashi, and the Kaiko-Nankai Scientific Crew (1992), Fluid venting activity within the Eastern Nankai trough accretionary wedge: A summary of the 1989 Kaiko-Nankai results, *Earth Planet. Sci. Lett.*, *109*(3–4), 303–318, doi:10.1016/0012-821X(92)90094-C.

Macgregor, D. S. (1993), Relationships between seepage, tectonics and subsurface petroleum reserves, *Mar. Pet. Geol.*, *10*, 606–619, doi:10.1016/0264-8172(93)90063-X.

Mamyrin, B. A., and I. N. Tolstikhin (1984), *Helium Isotope in Nature*, *Dev. Geochem.*, vol. 3, 273 pp., Elsevier, Amsterdam.

Marinaro, G., et al. (2006), Monitoring of a methane-seeping pockmark by cabled benthic observatory (Patras Gulf, Greece), *Geo Mar. Lett.*, *26*, 297–302, doi:10.1007/s00367-006-0040-4.

Marinaro, G., G. Etiope, F. Gasparoni, F. Furlan, and F. Bruni (2011), Gas seepage detection and monitoring at seafloor, paper presented at 10th Offshore Mediterranean Conference and Exhibition, Camera di Commer. Ravenna, Ravenna, Italy, 23–25 March.

Meade, B. J., B. H. Hager, S. C. McClusky, R. E. Reilinger, S. Ergintav, O. Lenk, A. A. Barka, and H. Ozener (2002), Estimates of seismic potential in the Marmara region from block models of secular deformation constrained by GPS measurements, *Bull. Seismol. Soc. Am.*, *92*, 208–215, doi:10.1785/0120000837.

Monteiro, P. M. S., A. van der Plas, V. Mohrholz, E. Mabille, A. Pascall, and W. Joubert (2006), Variability of natural hypoxia and methane in a coastal upwelling system: Oceanic physics or shelf biology?, *Geophys. Res. Lett.*, *33*, L16614, doi:10.1029/2006GL026234.

Muir-Wood, R., and G. C. P. King (1993), Hydrological signatures of earthquake strain, *J. Geophys. Res.*, *98*(B12), 22,035–22,068, doi:10.1029/93JB02219.

Newman, K. R., et al. (2008), Active methane venting observed at giant pockmarks along the U.S. mid-Atlantic

shelf break, *Earth Planet. Sci. Lett.*, *267*, 341–352, doi:10.1016/j.epsl.2007.11.053.

Parsons, T., S. Toda, R. S. Stein, A. A. Barka, and J. H. Dieterich (2000), Heightened odds of large earthquakes near Istanbul: An interaction-based probability calculation, *Science*, *288*, 661–665, doi:10.1126/science.288.5466.661.

Peters, K. E., C. C. Walters, and J. M. Moldowan (2004), *The Biomarker Guide*, vol. 1, *Biomarkers and Isotopes in the Environment and Human History*, 490 pp., Cambridge Univ. Press, Cambridge, U. K.

Polonia, A., et al. (2002), Exploring submarine earthquake geology in the Marmara Sea, *Eos Trans. AGU*, *83*(21), 229, doi:10.1029/2002EO000158.

Polonia, A., et al. (2004), Holocene slip rate of the North Anatolian Fault beneath the Sea of Marmara, *Earth Planet. Sci. Lett.*, *227*, 411–426, doi:10.1016/j.epsl.2004.07.042.

Ritt, B., J. Sarrazin, J.-C. Caprais, P. Noel, O. Gauthier, C. Pierre, P. Henry, and D. Desbruyeres (2010), First insights into the structure and environmental setting of cold-seep communities in the Marmara Sea, *Deep Sea Res., Part I*, *57*, 1120–1136, doi:10.1016/j.dsr.2010.05.011.

Sano, Y., and H. Wakita (1985), Geographical distribution of $^{3}He/^{4}He$ ratios in Japan: Implications for arc tectonics and incipient magmatsim, *J. Geophys. Res.*, *90*, 8729–8741, doi:10.1029/JB090iB10p08729.

Sugisaki, R., and K. Taki (1987), Simplified analysis of He, Ne and Ar dissolved in natural waters, *Chem. J.*, *21*, 21–23.

Tary, J. B., L. Géli, P. Henry, B. Natalin, L. Gasperini, M. Çomoğlu, and T. Bardainne (2011), Sea bottom observations from the western escarpment of the Sea of Marmara, *Bull. Seismol. Soc. Am.*, *101*, 775–791, doi:10.1785/0120100014.

Trique, M., P. Richon, F. Perrier, J. P. Avouac, and J. C. Sabroux (1999), Radon emanation and electric potential variations associated with transient deformation near reservoir lakes, *Nature*, *399*, 137–141, doi:10.1038/20161.

Weiss, R. F. (1974), Carbon dioxide in water and seawater: The solubility of a non-ideal gas, *Mar. Chem.*, *2*, 203–215, doi:10.1016/0304-4203(74)90015-2.

Wessel, P., and W. H. F. Smith (1998), New, improved version of generic mapping tools released, *Eos Trans. AGU*, *79*(47), 579, doi:10.1029/98EO00426.

Woodside, J. M., M. K. Ivanov, and A. F. Limonov (1998), Shallow gas and gas hydrates in the Anaximander Mountains region, eastern Mediterranean Sea, *Geol. Soc. Spec. Publ.*, *137*, 177–193, doi:10.1144/GSL.SP.1998.137.01.15.

Yang, T. F., D. R. Hilton, F. Italiano, and J. Heinicke (2010), Applications of fluid and gas geochemistry for geohazards investigation, *Appl. Geochem.*, *25*, 503–504, doi:10.1016/j.apgeochem.2010.01.007.

Zitter, T. A. C., et al. (2008), Cold seeps along the main Marmara fault in the Sea of Marmara (Turkey), *Deep Sea Res.*, *274*, 34–39.